Carbohydrate Research 426 (2016) 15–25

Contents lists available at ScienceDirect

Carbohydrate Research

journal homepage: www.elsevier.com/locate/carres

DFT/PCM theoretical study of the conversion of methyl 4-*O*-methyl-α-D-galactopyranoside 6-sulfate and its 2-sulfated derivative into their 3,6-anhydro counterparts

Vanina A. Cosenza, Diego A. Navarro, Carlos A. Stortz *

Departamento de Química Orgánica-CIHIDECAR, FCEyN-Universidad de Buenos Aires, Ciudad Universitaria, Buenos Aires 1428, Argentina

ARTICLE INFO

Article history:
Received 4 January 2016
Received in revised form 16 March 2016
Accepted 17 March 2016
Available online 21 March 2016

Keywords:
Alkaline treatment
3,6-Anhydrogalactose
Carrageenans
Conformation
Density functional theory
Galactose 6-sulfate

ABSTRACT

Modeling of the conversion of methyl 4-*O*-methyl-α-D-galactopyranoside 6-sulfate (**2**) and 2,6-disulfate (**1**) into methyl 3,6-anhydro-4-*O*-methyl-α-D-galactopyranoside (**4**) and its 2-sulfate (**3**), respectively (Scheme 1) has been carried out using DFT at the M06-2X/6–311 + G(d,p)//M06-2X/6–31 + G(d,p) level with the polarizable continuum model (PCM) in water. The three steps necessary for the alkaline transformation of 6-sulfated (and 2,6-disulfated) galactose units into 3,6-anhydro derivatives were evaluated. The final substitution step appears to be the rate limiting, involving an activation energy of ca. 23 kcal/mol. The other two steps (deprotonation and chair inversion) combined involve lower activation energies (9–12 kcal/mol). Comparison of the thermodynamics and kinetics of the reactions suggest that if the deprotonation step precedes the chair inversion, the reaction should be faster for both compounds. No major differences in reaction rate can be theoretically predicted to be caused by the presence of sulfate on O-2, although one experimental result suggested that O-2 sulfation should increase the reaction rate. The conformational pathways are complex, given the large number of rotamers available for each compound, and the way that some of these rotamers combine into some of the pathways. In any case, the conformation $^{O}S_{2}$ appears as a common intermediate for the chair inversion processes.

1. Introduction

Carrageenans are widely used as viscosants and gelling ingredients in the food and pharmaceutical industry. Their structures are based mainly on linear chains of alternating 3-linked β-D-galactopyranosyl residues and 4-linked α-D-galactopyranosyl residues. The α-linked residues may occur partly or totally as 3,6-anhydrogalactopyranosyl moieties.[1] These polysaccharides are usually substituted with sulfate ester groups and sometimes other substituents, and the whole sulfation pattern plus the presence or absence of 3,6-anhydrogalactose permits further classifications.[1] The last factor bears on the relationship with their industrial applicability, as non-gelling or weak gel-forming polysaccharides may be transformed into gelling ones by an alkaline aqueous modification, which increases the proportion of 3,6-anhydrogalactose. This reaction occurs only when 6-sulfated α-galactose moieties are present: heating the polysaccharide in strong alkaline medium generates an ionization (or polarization) of the 3-OH group, which further produces an intramolecular nucleophilic displacement of the sulfate group in position 6.[2–4] The reaction is atypical, as sulfate ester groups are usually stable in alkaline medium, given their low capacity as leaving groups.[5] In this way, it is highly specific, as only the 6-sulfate of 4-linked units is removed.[1] The reaction can be used at both the laboratory[3,4,6,7] and industrial scales to improve the gelling properties of carrageenans[1,4] as well as to the related agarans.[8]

For the galactose 6-sulfate moiety, the alkaline treatment reaction comprises three separate steps: (a) deprotonation of O-3, (b) chair flipping from $^{4}C_{1}$ to $^{1}C_{4}$, and finally (c) the actual $S_{N}2$ displacement. The order at which the first two steps occur is unknown, and thus they can be inverted. Ciancia and coworkers[4] have postulated that deprotonation should be the driving force, as it would lead to unstable contiguous negative charges (with deprotonated O-2 or with a 2-sulfate group) which would be alleviated by flipping into a $^{1}C_{4}$ conformation. However, no proof of this argument was given. The alkaline modification of galactans follows second-order kinetics, but at high NaOH concentrations, it becomes pseudo first-order[9] depending just on the concentration of galactose 6-sulfate. The half-lives at 80 °C, in 1M NaOH were highly dependent on the sulfation pattern of the β-galactose units: they ranged from a few minutes for 4-sulfated polysaccharides (κ-family),[4,10] to about 20–40 minutes in polysaccharides containing non-sulfated β-galactose units[11,12] and up to several hours for 2-sulfated polysaccharides (λ-family).[4] The presence of the sulfate group on O-2 of the α-galactose units seems to accelerate the reaction, as shown

* Corresponding author. Departamento de Química Orgánica-CIHIDECAR, FCEyN-Universidad de Buenos Aires, Ciudad Universitaria, Buenos Aires 1428, Argentina. Tel.: +54 11 45763346; fax: +54 11 45763346.
E-mail address: stortz@qo.fcen.uba.ar (C.A. Stortz).

http://dx.doi.org/10.1016/j.carres.2016.03.014
0008-6215/

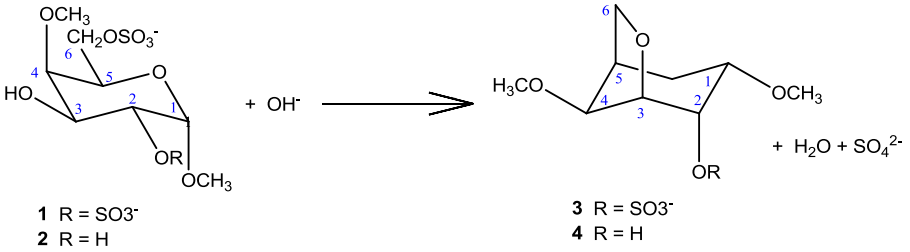

Scheme 1. Reaction and compounds under study.

by the comparison of ν- and μ/ν-carrageenans.[4,10] Microwave heating accelerates all the reactions, but maintains the differences between the distinct carrageenan types.[13]

Traditionally, due to their inherent complexity, modeling of carbohydrates has been carried out using different empirical force fields.[14,15] However, at the turn of the century, several quantum methods, as Hartree–Fock theory (HF) started to be applied to carbohydrates,[16] but rapidly switched to density functional theory (DFT),[17] especially using a hybrid functional like B3LYP.[18–21] Several studies have been carried out to compare the performance of different functionals for carbohydrates,[21–25] and concluded that B3LYP is not the best functional. From these results, the Minnesota new methods M05-2X[26] and M06-2X[27] emerged as best choices for carbohydrate studies.[25]

To gain further insight into the alkaline treatment reaction of red seaweed galactans, we undertook a complete modeling study of the conversion of methyl 4-*O*-methyl-α-D-galactopyranoside 6-sulfate (**2**) and 2,6-disulfate (**1**) into methyl 3,6-anhydro-4-*O*-methyl-α-D-galactopyranoside (**4**) and its 2-sulfate (**3**), respectively (Scheme 1), using DFT at the M06-2X/6–311 + G(d,p)//M06-2X/6–31 + G(d,p) level with the polarizable continuum model (PCM) in water[28] either assuming that deprotonation precedes chair inversion, or that, alternatively, chair inversion is the first step.

2. Methods

2.1. Calculations

Quantum mechanical (DFT) calculations were carried out using Gaussian 09W (Rev. B.01)[29] with the functional M06-2X,[27] the basis set 6–31 + G(d,p), the inclusion of water with the polarizable continuum model (PCM) and standard termination conditions for optimizations. Single point calculations at the M06-2X/6–311 + G(d,p) were also carried out, always including PCM in water. The appropriate chair rotamers were chosen by an exhaustive search using molecular mechanics calculations, carried out with MM3(92),[30] modified with sugar parameters as shown elsewhere.[31] For each chair used as starting structure, all the rotamers with energies within 2 kcal/mol above the minimum were submitted to the DFT calculations.

From the chosen chairs, separate conformational pathways were calculated for H(O)-3 protonated and deprotonated structures. Starting geometries for the different conformations were generated by modification of the different conformers previously modeled for 2-hydroxytetrahydropyran,[32] with the addition of the substituents with appropriate dihedral angles. Both minima and maxima were minimized directly using DFT calculation, in the later case, by the traditional Berny algorithm. When it was not possible to obtain the energy maximum by this algorithm, the QST2 procedure was employed.[33] Every transition state and intermediate for the chair conversion was searched for. For the final S_N2 step, the transition state was obtained by changing the distances between O-3–C-6 and C-6–O-6 and using the Berny algorithm. The final product of the reaction (3,6-anhydro derivative) was then minimized departing from the transition state and following the appropriate eigenvector.

Stationary points were optimized and later characterized by frequency calculations in order to verify that the minima and transition states have none and just one imaginary frequency, respectively. For the transition states, it was verified that this frequency corresponded to the conformational pathway searched for. Free energies were calculated at 298 K as reported in the Gaussian output file, without scaling. For the chair inversion, the progress of optimization of the transition states was followed in terms of the Cremer–Pople parameters,[34] in order to check for the appearance or disappearance of half-chair/envelope transition states with the different methods. The coordinates θ and ϕ were plotted in two hemispheres, which were drawn as azimuthal orthographic projections centered in the equator.[32] In the plot, circles represent minima (chairs or skews) and crosses represent maxima (half-chairs, envelopes and boats). The dashed lines are estimations of the pathways between two minima. The acidities on O-2 and O-3 were calculated by the same method, for the $^4C_1$ and $^1C_4$ conformations with less energy with and without the protons on O-2 and/or O-3.

2.2. Nomenclature

The orientations of exocyclic groups in **1–2** are indicated by χ_n, defined by the atoms H-*n*–C-*n*–O-*n*–X, for *n* = 1 to 4, where the substituent X is methyl for *n* = 1 and 4, hydrogen for *n* = 2 (in **2**) or 3 (in **1** and **2**) and sulfate for *n* = 2 in **1**. The angle χ_6 is defined by atoms C-5–C-6–O-6–S, and ω is defined by atoms O-5–C-5–C-6–O-6. When **1** and **2** are H(O)-3 deprotonated, they are named as **1d** and **2d**, respectively, and χ_3 has no value. In **3** and **4**, the only angles that can be defined are χ_n with *n* = 1, 2 or 4. The values of all those angles are described by a one-letter code:[35] **S** for angles between –30° and +30°, **g** for 30–100°, **T** for angles with absolute value larger than 150°, **G** for angles between –30° and –100°, **e** for angles between 100 and 150°, and **E** for angles between –100° and –150°.

3. Results and discussion

3.1. The alkaline treatment reaction. Conformational pathways of pyranosides

The reaction under study (Scheme 1) has, as its last step, a nucleophilic attack of the deprotonated O-3 over C-6, with formation of a strained 3,6-anhydro ring and a final loss of sulfate.[2–4] However, in order to have the attacking O-3 close to the electrophilic C-6, the galactopyranose chair should switch from its usual $^4C_1$ conformation to the more strained $^1C_4$ conformation, *i.e.* it should undergo chair inversion. This process requires overriding a half-chair-like transition state to get to the boat-skew region, from which another transition state must be overstepped to arrive at the inversed chair. This process is relatively simple in cyclohexane, due to its symmetry: both chairs and all 6 boats, skews, half chairs and envelopes

Table 1
Geometries and relative energies[a] of selected rotamers of **1** and **1d** after calculation with M06-2X/6–31 + G(d,p) including PCM in water

Rotamer	χ_1 (°)	χ_2 (°)	χ_3 (°)	χ_4 (°)	ω(°)	χ_6 (°)	ΔG (kcal/mol)[a] (kcal/mol)
1-$^4C_1$							
a (χ_3 = **g**, χ_4 = **g**)	–54	10	97	32	70	–173	0.00
1-$^1C_4$							
a (χ_3 = **G**, χ_4 = **G**)	–49	22	–68	–50	59	–144	0.00 (5.48)[b]
b (χ_3 = **G**, χ_4 = **g**)	–50	21	–76	49	61	–165	0.44
c (χ_3 = **g**, χ_4 = **g**)	–49	22	43	56	62	–161	1.69
d (χ_3 = **g**, χ_4 = **G**)	–50	23	42	–51	61	–167	2.00
1d-$^4C_1$							
a (χ_4 = **g**)	–55	–25	-	28	71	–172	0.00[c]
1d-$^1C_4$							
a (χ_4 = **g**)	–50	17	-	60	63	–164	0.00 (2.03)[b]
b (χ_4 = **G**)	–50	17	-	–52	62	–168	0.56

[a] For each chair, the lower-energy conformer is considered as energy zero.
[b] In parentheses, the ΔG relative to the corresponding $^4C_1$ is shown.
[c] ΔG (**1**-$^4C_1$ + OH^- → **1d**-$^4C_1$ + H_2O) = –0.33 kcal/mol.

are equivalent.[32,36] In cyclohexane, the chair is the global minimum (most stable conformer), whereas the skew is a local minimum, the boat is a transition state between skews, and the half chair is a transition state between chair and skew. Although the skew represents an energy minimum and the boat an energy maximum, the difference in energy between both is small, and thus an easy pseudorotational circuit is established between boats and skews. When cyclohexane is substituted, the symmetry is lost partially or totally.[32,36]

Conformations of six-membered rings can be described with spherical coordinates similar to the Earth's latitude and longitude,[37,38] as well as a radius that indicates the magnitude of puckering *Q*. In the frequently used Cremer–Pople system,[34] the puckering parameters are, besides *Q*, ϕ (0 to 360°, longitude) and θ (0 to 180°, latitude). Spherical polar coordinates are usually employed for the representation of conformers, considering the conformers to lie on an even external shell of the sphere of constant radius *Q* (although actually the radius is not constant, even for ideal conformations). The chairs appear on the poles (θ = 0 and 180°, ϕ irrelevant), whereas the pseudorotational path of skews and boats appears on the equator (θ = 90°), each conformer being distinguished by its ϕ value. Perfect half-chairs come out at θ = 50.9 and 129.1°. In order to produce a 2-dimensional representation, several approaches have been made. In this work, the Cremer–Pople parameters on each hemisphere are drawn as an azimuthal orthographic projection centered in the equator. Due to the lack of symmetry, both hemispheres have to be shown.[32]

3.2. Molecular modeling of the conversion 1 → 3

Compound **1** (Scheme 1) carries a sulfate group on O-2. This substitution has the advantage of restricting the number of allowed rotamers of **1**. The sulfur atom always tends to stay more or less eclipsed with H-2. A full search of conformers for the $^4C_1$ and $^1C_4$ chairs of **1** and of **1d** (*i.e.***1** deprotonated on O-3) was carried out using MM3 (see Section 2). Those with energies within 2 kcal/mol of the minimum for each shape were submitted to a DFT/PCM (water) calculation at the M06-2X/6–31 + G(d,p) level. The resulting conformers are shown in Table 1. It is noteworthy that although some conformers with ω ≈ 180° appear within the upper limit of energy, they were not taken into account in the current modeling as this conformation is unable to allow the final substitution step. For the S_N2 to occur, ω has to bear an angle of ca. 90°, close to that obtained in the lower energy conformers shown on Table 1.

In Table 1, all the conformers have χ_1 = **G** as expected from the exo-anomeric effect, χ_2 = **S** due to the size of the sulfate group, ω = **g** and χ_6 = **T**. The only exocyclic angles that present variations are χ_3 and χ_4. However, for the $^4C_1$ chair, χ_4 should be gauche positive (**g**), as other conformation would lead to sterical conflict between the *O*-methyl group on C-4 and the large substituent on C-5. This means that only one $^4C_1$ conformer is possible for **1d**. For compound **1**, although three conformers could possibly appear, the hydrogen bond-like interaction between H(O)-3 and O(S)-2 strongly stabilizes the rotamer with χ_3 = **g**. Attempts to optimize a conformer with χ_3 = **T** converge with those leading to χ_3 = **g**, *i.e.*, only one conformer of this chair is obtained within the chosen energy range (Table 1). More conformers can be obtained for the $^1C_4$ conformers. However, in order to establish the full path of the reaction, the single possible starting point is conformer a of **1**, to lead to **3** with χ_4 = **g**. The only way to arrive to a conformer of **3** with χ_4 = **G** comes from a rotation of the substituent over C-4 in the $^1C_4$ conformer (**1** or **1d**) from **g** to **G**. Thus, the full reaction **1** → **3** can be depicted in Scheme 2.

Two different pathways were calculated: one where the chair inversion comes first, followed by deprotonation, and another one where deprotonation is the first step, followed by chair inversion. The energies and steps corresponding to those paths are shown in Fig. 1 (chair inversion/deprotonation) and 2 (deprotonation/chair inversion). For the first variant (Fig. 1), the pathway from the most stable chair to the equator requires an activation energy of about 12 kcal/mol, by two different transition states ($^4H_3$ and $^OH_1$). Along

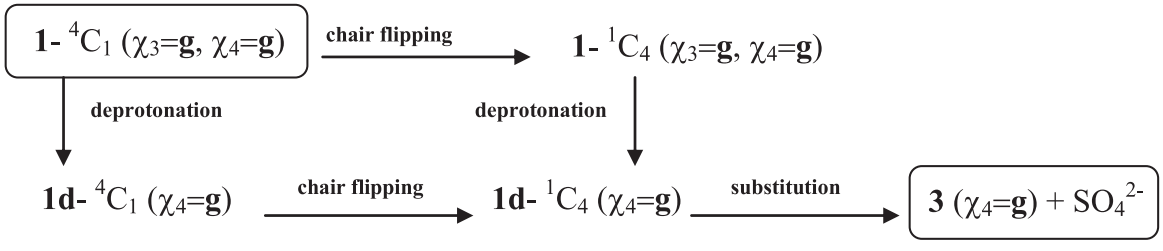

Scheme 2. Pathways for the alkaline conversion of **1** to **3**.

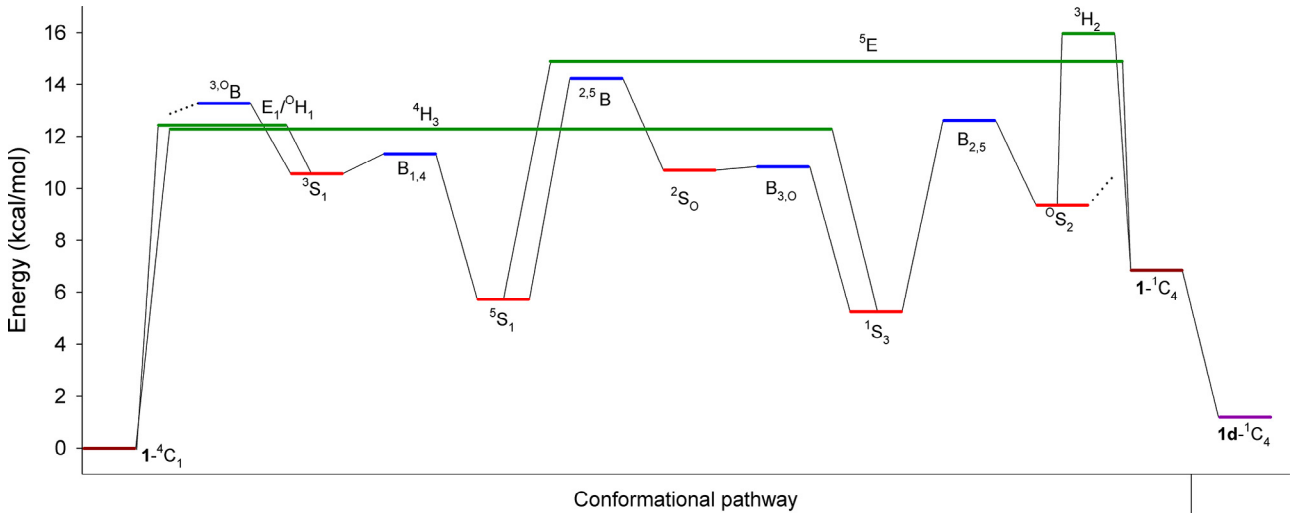

Fig. 1. Conformational pathway for the chair inversion of **1**, with energies calculated at the M06-2X/6–311 + G(d,p) level and geometries calculated at the M06-2X/6–31 + G(d,p) level, both with the polarizable continuum method in water. The pathway around the equator is circular. The deprotonation step is included at the right.

the equator, there are some very stable skew conformations like $^{5}S_1$ and $^{1}S_3$, stabilized by a hydrogen bond between H(O)-3 and O(S)-2, even more stable than the $^{1}C_4$ conformation. From these equatorial conformers, a second barrier (there are two alternatives) of about 9 kcal/mol has to be overstepped to reach the alternate chair, $^{1}C_4$ (Fig. 1). This chair easily losses a proton in an exothermic reaction (in alkaline medium) to generate the starting point of the substitution reaction. The alternative pathway, depicted in Fig. 2, requires a first step of deprotonation. This step is also slightly exothermic. From this deprotonated chair, the pathway to the equator has an energy barrier of about 11 kcal/mol (Fig. 2). The pseudorotational pathway around the equator is partially hindered by the large instability of the boat form $^{2,5}B$. In any case, the equatorial conformation $^{O}S_2$ can flip to the adequate chair ($^{1}C_4$) through the transition state $^{3}H_2$, with an activation energy of about 5 kcal/mol. The comparison of the two alternative pathways suggests a kinetic preference for the second one, *i.e.* deprotonation as the first step of the reaction, at least when a sulfate is present on O-2. The energy barriers are lower in this case, especially the last step. The thermodynamics also seem to favor the second process: the energy difference between the $^{4}C_1$ and $^{1}C_4$ forms of **1** are larger than those in **1d**. This agrees with the assertion of Ciancia et al[4] regarding the "instability" of the deprotonated $^{4}C_1$ conformer by its neighboring negative charge on O-2, leading more easily to a chair inversion. Anyway, the substitution step is rate-limiting, with an activation energy of 23.1 kcal/mol (see Section 3.4).

Fig. 3 shows the representation of the stationary points and conformational pathways for the chair inversion of **1** and **1d**, studied at the M062X/6–31 + G(d,p) level, using the Cremer–Pople parameters drawn as an azimuthal orthographic projection centered in the equator. Fig. 3a shows two different pathways for **1**, regarding the passage $^{4}C_1 \rightarrow$ equator, and other two for the passage equator $\rightarrow {}^{1}C_4$, one on each hemisphere. For **1d**, Fig. 3b shows the only possible pathway for each passage that we have found. Full passage requires further steps around the equator. The two half-chair transition states existing for **1d** ($^{4}H_3$ and $^{3}H_2$) also appear for **1**, but in this case, two additional transition states appear (^{5}E and $^{O}H_1$).

3.3. Molecular modeling of the conversion 2 → 4

As compound **2** has an hydroxyl group on O-2, its rotation generates more possible starting conformers. The stability of the different structures is partially driven by possible hydrogen bonds between H(O)-3 with O-4 or O-2, and of H(O)-2 with O-3 or O-1. The full

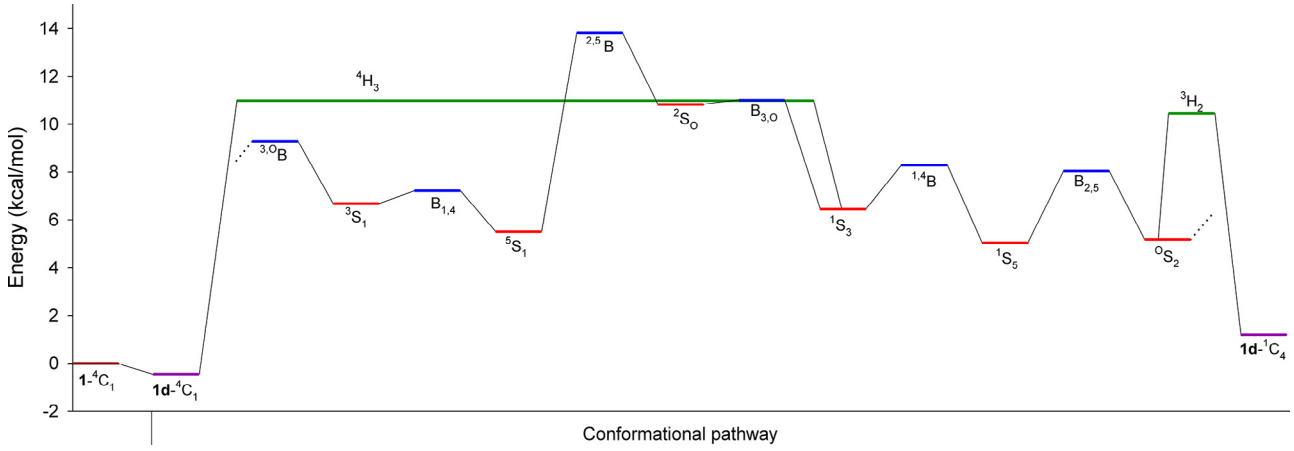

Fig. 2. Conformational pathway for the chair inversion of **1d**, with energies calculated at the M06-2X/6–311 + G(d,p) level and geometries calculated at the M06-2X/6–31 + G(d,p) level, both with the polarizable continuum method in water. The pathway around the equator is circular. The deprotonation step is included at the left.

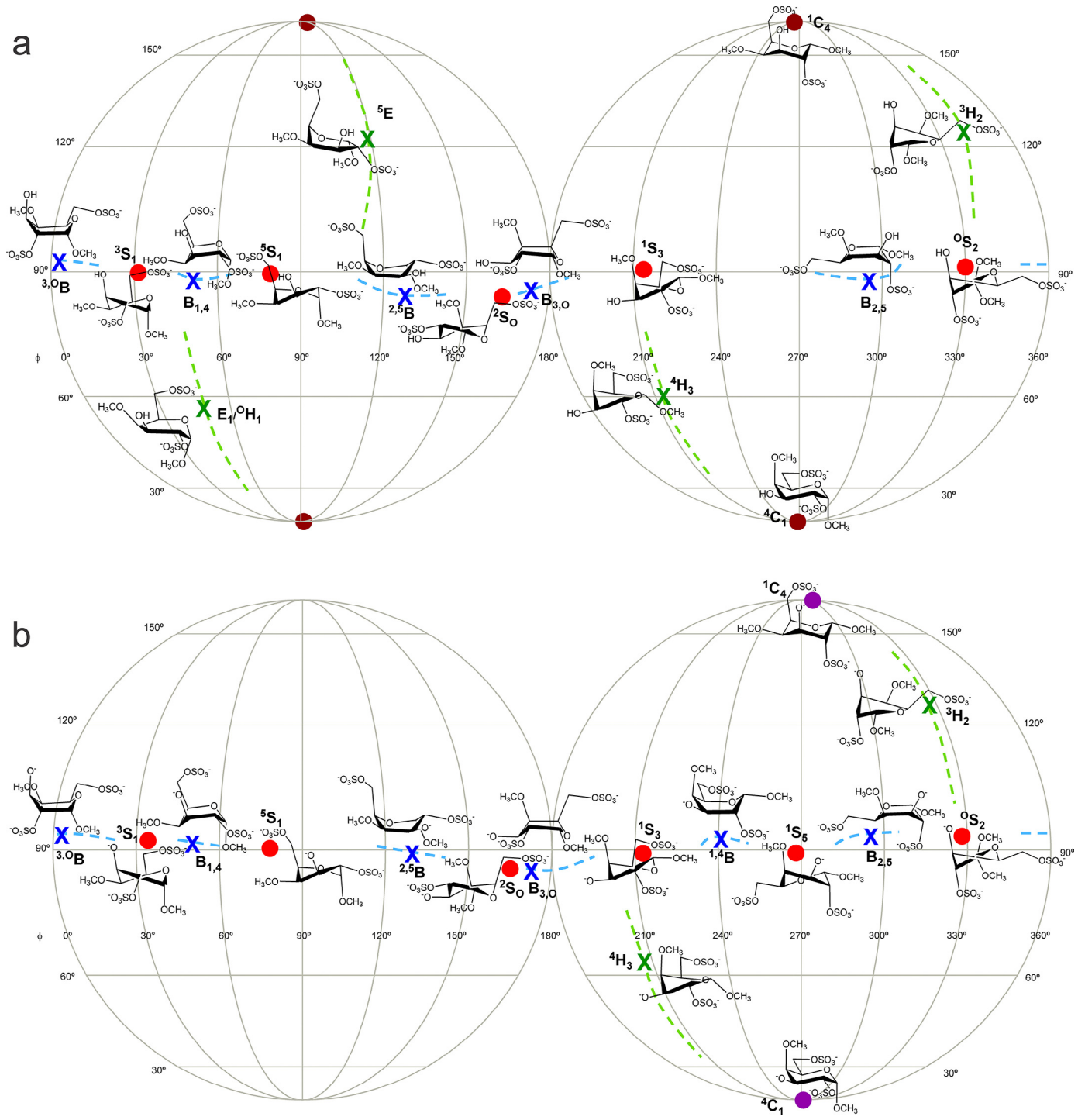

Fig. 3. Geometry representations of the Cremer–Pople puckering parameters in an azimuthal orthogonal projection (centered on the equator) for the complete conformational pathway for compounds **1** (a) and **1d** (b), at the M06-2x/6–31 + G(d,p) level with the polarizable continuum method in water. Circles represent minima (chairs and skews), crosses represent transition states (half-chairs, envelopes and boats), and dashed lines represent the approximate pathways. The exocyclic dihedral angles may vary during the pathway.

search with MM3 followed by DFT/PCM calculations, leaving out the conformers with high energy, as carried out for **1**, yielded the results shown on Table 2.

As occurred with **1**, rotamers with ω = **g** and χ_6 = **T/E** are the most stable, and the $^{4}C_{1}$ conformations cannot occur with χ_4 = **G** because of the sterical hindrance with the substituents on C-5. The table includes some conformers with energies well beyond the 2 kcal limit; they were included because the corresponding inverted chair is very stable. Thus, in order to look at the complete pathways, they should be included. In some pathways, rotation around exocyclic angles is produced. Thus, the pathways are not "clean", but they combine themselves in paths with common skew, boat or half-chair conformations. After a complete analysis of the conformers involved starting from the eight different rotamers of **2** in its normal chair form, it has been concluded that the possible reaction pathways are those shown on Scheme 3.

Table 2
Geometries and relative energies[a] of selected rotamers of **2** and **2d** after calculation with M06-2X/6–31 + G(d,p) including PCM in water

Rotamer	χ_1 (°)	χ_2 (°)	χ_3 (°)	χ_4 (°)	ω(°)	χ_6 (°)	ΔG (kcal/mol)[a] (kcal/mol)
2-$^4C_1$							
a (χ_2 = **T**, χ_3 = **T**, χ_4 = **S**)	–55	–168	–169	–16	66	–172	0.00
b (χ_2 = **T**, χ_3 = **g**, χ_4 = **g**)	–54	–165	71	34	69	–173	0.13
c (χ_2 = **g**, χ_3 = **T**, χ_4 = **S**)	–55	71	–166	–18	66	–172	0.52
d (χ_2 = **T**, χ_3 = **G**, χ_4 = **g**)	–55	–166	–42	30	68	–173	1.74
e (χ_2 = **G**, χ_3 = **g**, χ_4 = **g**)	–55	–38	72	34	69	–173	1.81
f (χ_2 = **G**, χ_3 = **T**, χ_4 = **S**)	–55	–46	–168	–17	66	–171	1.92
g (χ_2 = **g**, χ_3 = **G**, χ_4 = **g**)	–55	71	–38	32	69	–174	2.05
h (χ_2 = **G**, χ_3 = **G**, χ_4 = **g**)	–56	–46	–41	30	69	–172	3.84
2-$^1C_4$							
a (χ_2 = **G**, χ_3 = **G**, χ_4 = **G**)	–54	–78	–69	–51	58	–141	0.00 (2.93)[b]
b (χ_2 = **G**, χ_3 = **G**, χ_4 = **g**)	–53	–78	–76	40	61	–138	0.30
c (χ_2 = **E**, χ_3 = **G**, χ_4 = **G**)	–52	–147	–68	–49	56	–145	1.03
d (χ_2 = **E**, χ_3 = **G**, χ_4 = **g**)	–51	–149	–76	40	55	–149	1.39
e (χ_2 = **G**, χ_3 = **g**, χ_4 = **g**)	–53	–77	47	51	60	–137	1.92
f (χ_2 = **g**, χ_3 = **G**, χ_4 = **G**)	–49	45	–68	–50	58	–145	2.46
g (χ_2 = **E**, χ_3 = **g**, χ_4 = **g**)	–51	–148	47	58	52	–149	2.68
h (χ_2 = **g**, χ_3 = **G**, χ_4 = **g**)	–50	44	–75	38	58	–169	2.98
2d-$^4C_1$							
a (χ_2 = **g**, χ_4 = **g**)	–55	86	-	35	68	–174	0.00[c]
b (χ_2 = **T**, χ_4 = **g**)	–56	–175	-	33	68	–172	3.32
c (χ_2 = **G**, χ_4 = **g**)	–56	–54	-	33	68	–172	5.76
2d-$^1C_4$							
a (χ_2 = **G**, χ_4 = **g**)	–53	–77	-	62	62	–155	0.00 (4.68)[b]
b (χ_2 = **G**, χ_4 = **G**)	–54	–76	-	–51	67	–160	0.39
c (χ_2 = **T**, χ_4 = **g**)	–51	–155	-	59	58	–168	0.62
d (χ_2 = **T**, χ_4 = **G**)	–50	–153	-	–51	63	–162	1.11
e (χ_2 = **g**, χ_4 = **g**)	–50	76	-	59	59	–168	1.66
f (χ_2 = **g**, χ_4 = **G**)	–50	76	-	–51	65	–161	2.07

[a] For each chair, the lower-energy conformer is considered as energy zero.
[b] In parentheses, the ΔG relative to the corresponding $^4C_1$ is shown.
[c] ΔG (**2**-$^4C_1$ conf.a + OH^- → **2d**-$^4C_1$ conf.a + H_2O) = –5.51 kcal/mol.

The pathways were considered disregarding the possibility of deprotonation on O-2. Actually, it has been calculated that the H(O)-2 is slightly more acidic than H(O)-3 (ΔG = –5.84 vs –5.24 kcal/mol for the $^4C_1$ form). However, our calculations also indicate that double deprotonation is less likely to occur (ΔG = +5.12 kcal/mol, more than +10 kcal starting from singly deprotonated species), and thus only the effect of single deprotonation on O-3, necessary for the substitution step, was modeled. It is noteworthy that for the $^1C_4$ form, the relative acidities reverse (ΔG = –2.72 for O-2 and –3.58 kcal/mol for O-3).

The analysis of Scheme 3 indicates that for the eight $^4C_1$ conformers of **2**, pathways starting with the chair inversion can be established. However, some of these pathways crossover between themselves, as only four different conformers of **4** can be obtained. On the other hand, there are five conformers of **2** that can undergo deprotonation first, to give **2d**, and then go on to a further chair inversion (by one of three different paths) and substitution to arrive at **4**. As stated previously, deprotonation appears to be thermodynamically favored (i.e. H(O)-3 is more acidic than water). Furthermore, it is more favored in the $^4C_1$ chair than in the $^1C_4$ chair (see above). The energies and geometries involved in the pathways starting from some **2d** conformers (i.e. deprotonation first) are shown in Fig. 4, whereas the corresponding pathways on spherical coordinates are shown in Fig. 5. Fig. 4 shows two different

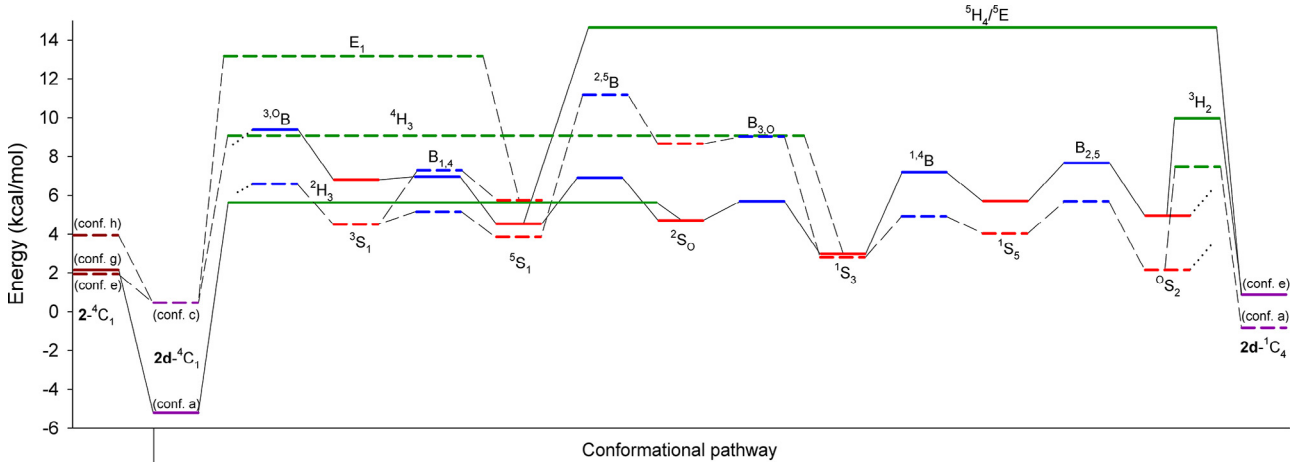

Fig. 4. Conformational pathway for the chair inversion of **2d**, with energies calculated at the M06-2X/6–311 + G(d,p) level and geometries calculated at the M06-2X/6–31 + G(d,p) level, both with the polarizable continuum method in water. Full line, conformer with χ_2 = g; dashed line, conformer with χ_2 = T/G. The pathway around the equator is circular. The deprotonation step is included at the left.

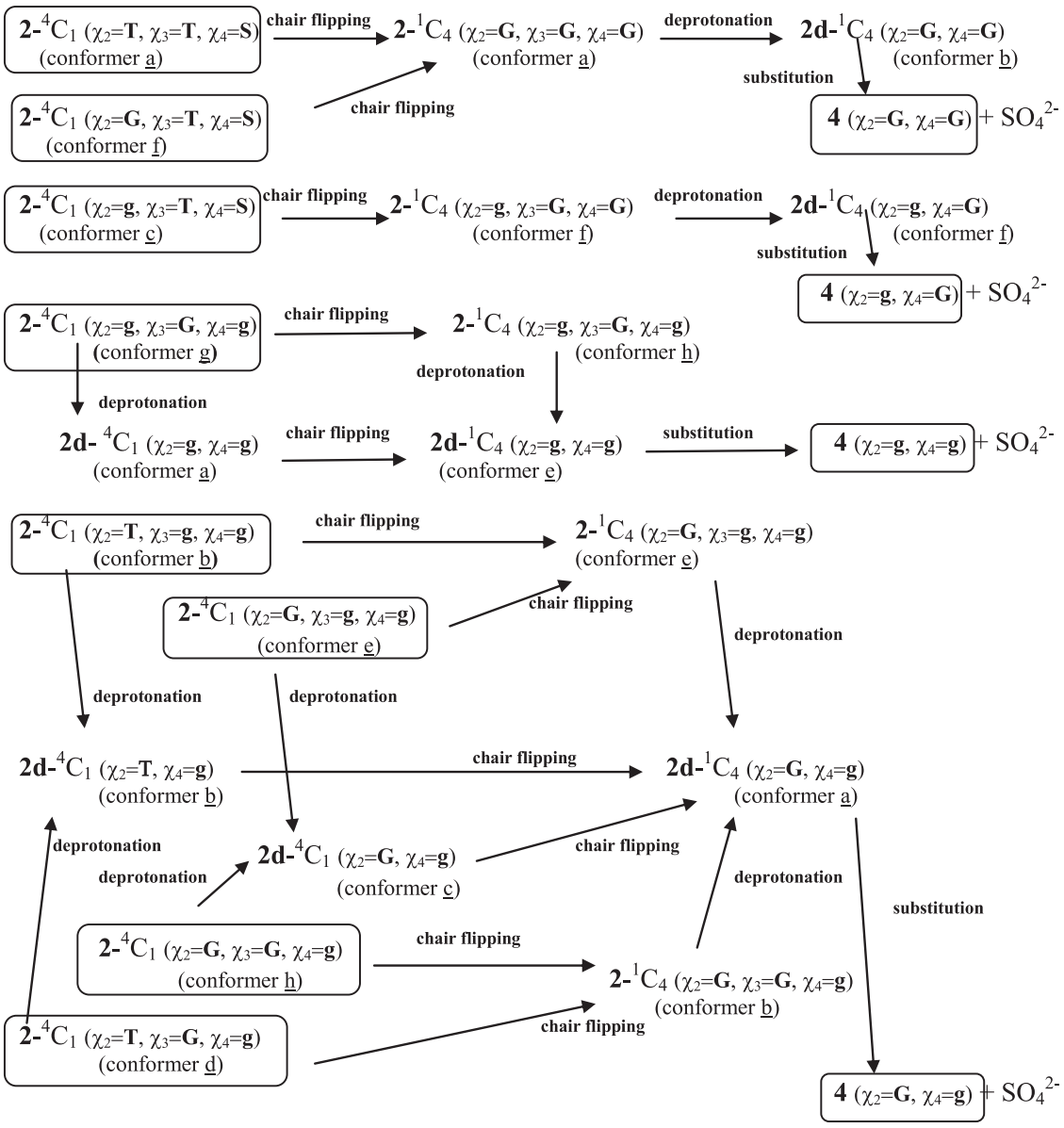

Scheme 3. Pathways for the alkaline conversion of **2** to **4**.

pathways: one starts from conformer a ($^4C_1$) of **2d**, generated by deprotonation of conformer g of **2**. The half chair $^2H_3$ serves as transition state to the equator, with a low energy barrier (ca. 10 kcal/mol). Furthermore, its energy is about the same as the lower-energy skew-boats. From the equator into the $^1C_4$ conformation there are two possible pathways (Fig. 5a): the one with the lower energy involves passage through the $^3H_2$ half chair; the other one, through the $^5H_4$ conformation involves a higher energy. The other pathway shown in Fig. 4 involves conformer c ($^4C_1$) of **2d**, generated from two different conformers of **2** (e and h), having $\chi_2 = \mathbf{G}$. Although this pathway can be completed by one side of the pseudorotational equatorial way, to be fully available (i.e. generate the $^{2,5}B$ conformation) requires rotation to $\chi_2 = \mathbf{T}$ (Fig. 5b). The last pathway (not shown), corresponding to conformer b of **2d** ($\chi_2 = \mathbf{T}$) shows some independent conformers, but in order to get to the inverted chair, it needs forcedly to rotate χ_2 and thus combine with the pathway shown (Fig. 5b). The energy barriers involved are quite low: about 9 kcal/mol to pass through the half chair $^4H_3$ (and quite a bit more through E_1), and even less to get to the inverted chair through the half chair $^3H_2$. Furthermore, in this pseudorotational cycle, the barrier to obtain the conformer $^1C_4$ is lower than that to recover the $^4C_1$.

On the other hand, there are several different pathways that start with the chair inversion (Scheme 3). Many of them mix up in some part of the pathway through rotation of some of the exocyclic angles. A careful look at the energies involved in the chair inversion indicate energies of about 10–15 kcal/mol for the first barrier, and usually a similar or higher barrier for the second step, which leads to the $^1C_4$ conformation. Fig. 6 shows the energies and geometries involved for the lower energy conformer of **2** (a, $^4C_1$), which lead, after rotation of the three exocyclic groups, to the lower energy alternate chair (a, $^1C_4$), as an example. The remaining pathways are shown as Supplementary Material. In the example, E_1 is the transition state from the $^4C_1$ conformer (with an energy about 13 kcal/mol above), and $^3H_2$ the transition state to the $^1C_4$ chair. Fig. 7 shows the geometries involved in the pathway. The comparison of the results of the two alternative ways (deprotonation → inversion or inversion → deprotonation) suggests that, as occurred for **1**, the deprotonation as first step appears to be favored.

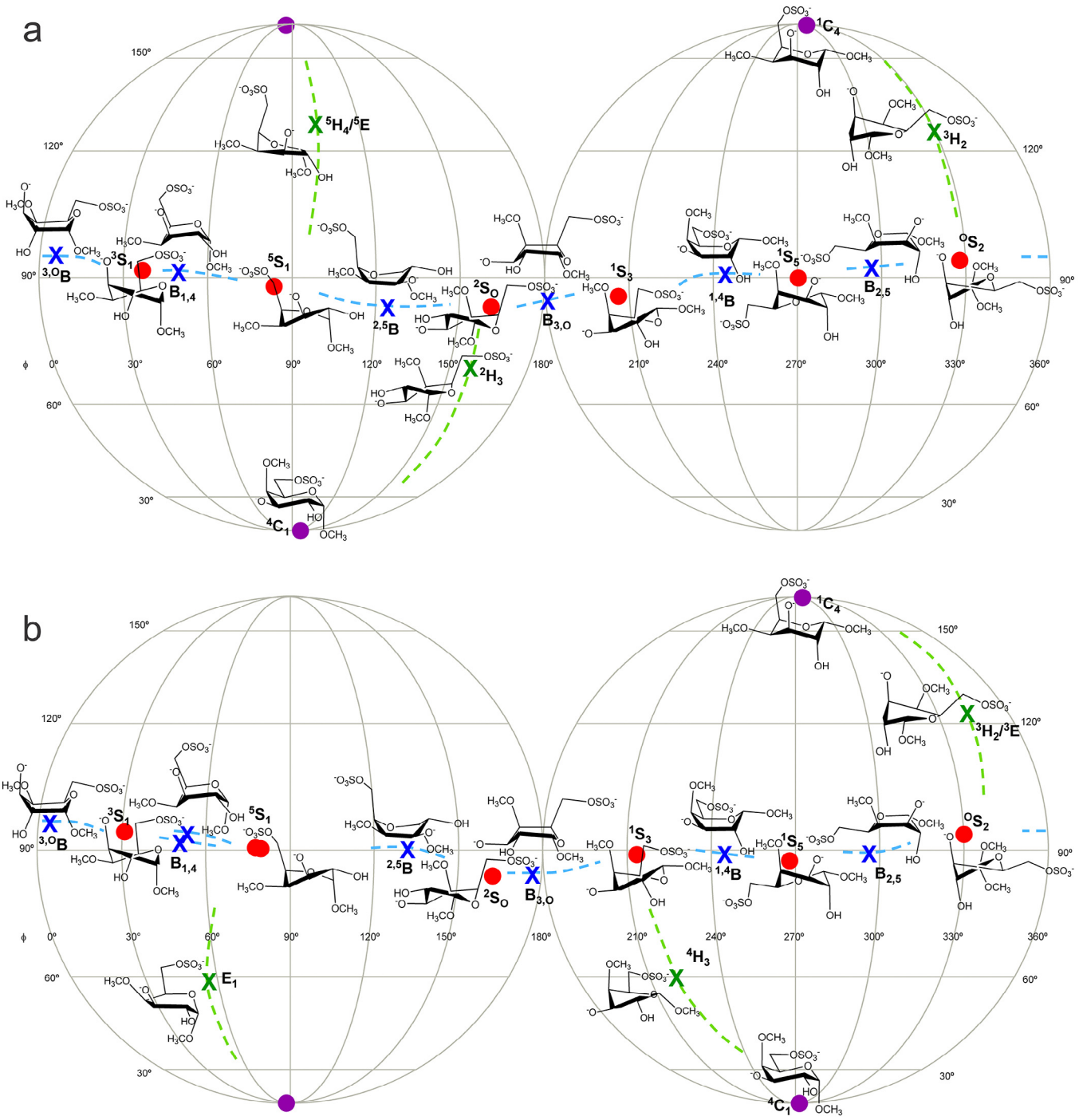

Fig. 5. Geometry representations of the Cremer–Pople puckering parameters in an azimuthal orthogonal projection (centered on the equator) for the complete conformational pathway for compound **2d,** conformer a (a) and conformer c (b), at the M06-2x/6–31 + G(d,p) level with the polarizable continuum method in water. Circles represent minima (chairs and skews), crosses represent transition states (half-chairs, envelopes and boats), and dashed lines represent the approximate pathways. The exocyclic dihedral angles may vary during the pathway.

3.4. Substitution step

The final step of the whole reaction is the S_N2-like reaction, which involves an attack of the deprotonated O-3 (in **1d** and **2d**) over C-6 to form a transition state with a trigonal C-6 with O-3 and the OSO_3^- groups overlapping both lobes of the *p* orbital. Fig. 8 shows one of those transition states. The O-C-O distances suggest an early transition state (reagent-like). This step is by far the rate-limiting step. The energies involved in this step are shown in Table 3. No major variations are observed between different compounds, or between different conformers of a compound. However, for the later comparison, it appears that kinetically favored pathways are also thermodynamically favored. For the most favored transformation for each compound, it is shown that the conversion of **2d** is favored over that of **1d** by about 0.4 kcal/mol, both thermodynamically and kinetically, an almost negligible difference. The conformational changes and deprotonation also show similar differences, favoring slightly the conversion of **2d**. This seems to contradict the only

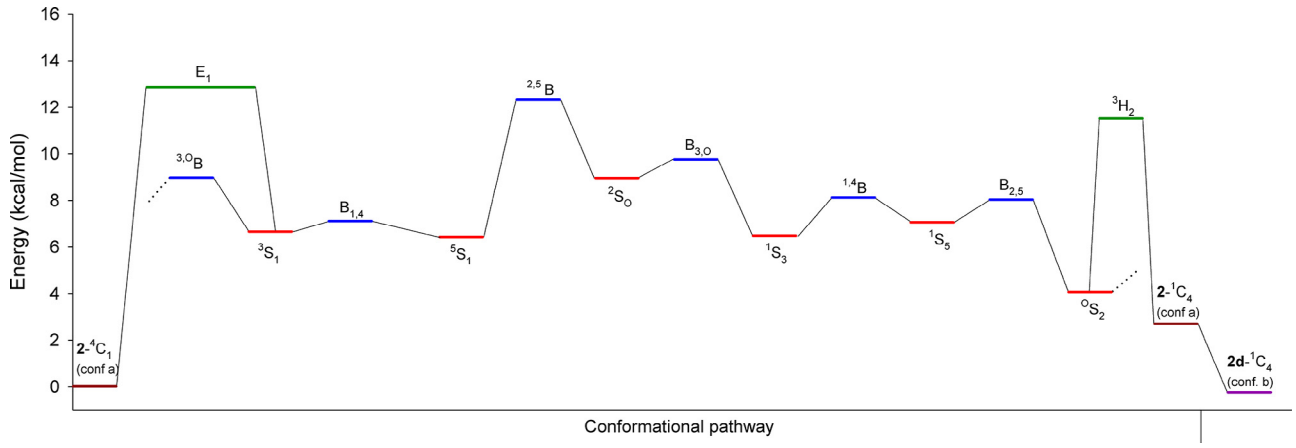

Fig. 6. Conformational pathway for the chair inversion of **2**, conformer a, with energies calculated at the M06-2X/6–311 + G(d,p) level and geometries calculated at the M06-2X/6–31 + G(d,p) level, both with the polarizable continuum method in water. The pathway around the equator is circular. The deprotonation step is included at the right.

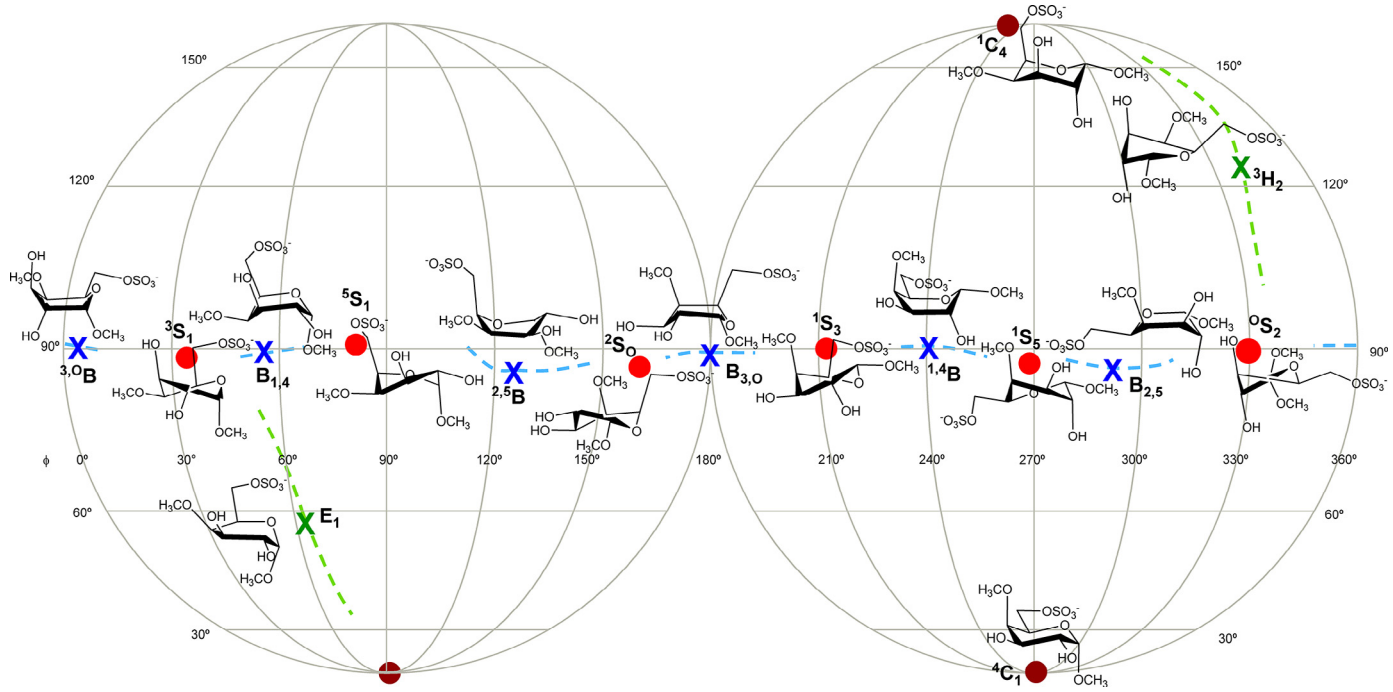

Fig. 7. Geometry representations of the Cremer–Pople puckering parameters in an azimuthal orthogonal projection (centered on the equator) for the complete conformational pathway for compound **2**, conformer a, at the M06-2x/6–31 + G(d,p) level with the polarizable continuum method in water. Circles represent minima (chairs and skews), crosses represent transition states (half-chairs, envelopes and boats), and dashed lines represent the approximate pathways. The exocyclic dihedral angles may vary during the pathway.

experimental data, which suggests that sulfation on O-2 accelerates the reaction. However, this reaction has been made just once, with a mixture of μ- and ν-carrageenans. The use of standards enriched in those structures is needed to ascertain if this trend can be proved experimentally.

3.5. The chair/half chair/boat/skew boat conformational pathway

Cyclohexane has a conformational pathway with two equivalent chairs, twelve equivalent half chairs linking the pole area from the equator, and at this point, six skew boats representing minima

Table 3
Activation energies ($\Delta G^{\neq}$) and reaction energies (ΔG) for the substitution step of different conformers of **1d** and **2d**, leading to **3** and **4**, respectively

Reaction	$\Delta G^{\neq}$ (kcal/mol)[a]	ΔG (kcal/mol)[a]
1d (χ_4 = **g**) → **3** (χ_4 = **g**)	23.10	–16.67
1d (χ_4 = **G**) → **3** (χ_4 = **G**)	22.61	–18.45
2d (conf. a) → **4** (χ_2 = **G**,χ_4 = **g**)	22.82	–16.98
2d (conf. b) → **4** (χ_2 = **G**,χ_4 = **G**)	22.23	–18.82
2d (conf. e) → **4** (χ_2 = **g**,χ_4 = **g**)	23.70	–15.81
2d (conf. f) → **4** (χ_2 = **g**,χ_4 = **G**)	23.03	–17.27

[a] At the M06-2X/6–311 + G(d,p)//M06-2X/6–31 + G(d,p) level, both including PCM in water.

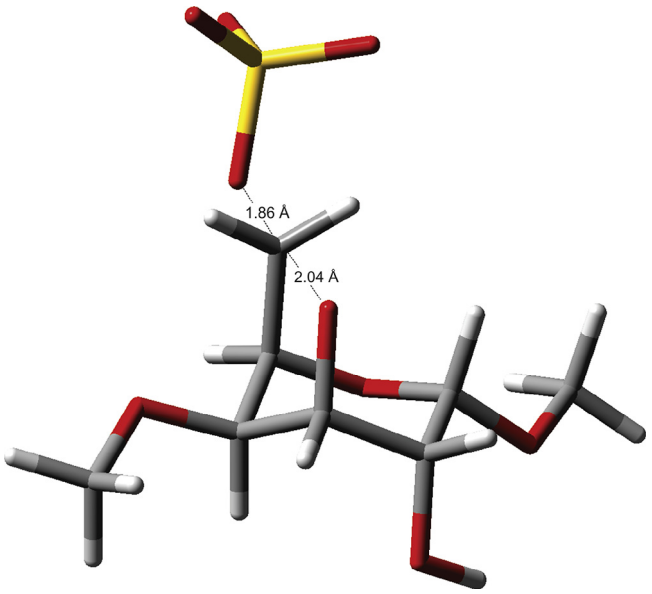

Fig. 8. Structure of the transition state for the substitution step of **2d** (conformer a) →**4**, with selected distances shown.

of energy and six boats representing energy maxima.[32] Simply substituted cyclohexanes show a similar map, but showing less symmetry and thus, some allowed skew boats and some forbidden.[32] The half chairs are usually 10–12 kcal/mol above the most stable chair, and the skew boats ca. 7 kcal/mol above those chairs. When it comes to 2-hydroxytetrahydropyran, the simplest model of a pyranosic sugar, the relative energies are modified. A previous work showed half chair energies of less than 9 kcal/mol, and a skew boat ($^{O}S_2$) especially stabilized by the anomeric effect at about 4 kcal/mol. The boat $^{1,4}B$ is especially unstable, about the same as the half chairs.[36] Other skew boats as $^{5}S_1$ and $^{3}S_1$ have also low energy (less than 5 kcal/mol).[32,36,39] Other authors have found similar results, although Stortz found four skew boats, Smith[39] has found all the six, and Ionescu et al[36] has found five.

First attempts to extend these studies to actual pyranosic sugars were carried out using empirical (molecular mechanics) methods.[40,41] As happened with the simplest model, the skew boats $^{1}S_3$ and $^{O}S_2$ are the most stable conformers in the equator for pyranoses with the *gluco* and *galacto* configuration,[41] with energies ca. 7 kcal/mol larger than the most stable chair for $^{1}S_3$. Using quantum methods for five different pyranosic sugars, Mayes et al[42] have also determined that $^{1}S_3$ and $^{O}S_2$ are the most stable conformers in the equatorial area, within a very complex crossway of paths. A metadynamics study confirmed these two skew boats (or similar conformations) as the most stable for glucopyranoses,[43] but also included $^{1}S_5$ for mannopyranoses.[44] A more recent study confirmed that conformations close to $^{1}S_3$ and $^{O}S_2$ are the most stables for glucopyranoses and are those more likely to mediate in the chair inversion processes.[45]

In the present study, the sulfate and methyl groups could change the usual pathway. For the conformational inversion of **1**, $^{1}S_3$ and $^{5}S_1$ appear as the most stable skew boats (ca. 5 kcal/mol), whereas $^{O}S_2$, $^{3}S_1$ and $^{2}S_O$ are less stable (ca. 10 kcal/mol, Fig. 1). Deprotonation levels the energies of the skew boat conformers (Fig. 2). Thus, $^{5}S_1$, $^{1}S_5$ and $^{O}S_2$ appear 5 kcal/mol above the most stable conformer of **1d**, and the remaining three skew boats also appear, although with higher energies. In both cases, conformation $^{1}S_3$ appears as the conformation connected with $^{4}C_1$, whereas $^{O}S_2$ appears connected with the inverted chair (Fig. 3). For the inversion of **2**, although each exocylic rotamer exhibits a different pathway, all of them show $^{O}S_2$ as the most stable skew boat conformer (Fig. 6), and acting as intermediate toward the $^{1}C_4$ conformation (Fig. 7). The intermediates connected to the $^{4}C_1$ conformation are different for each rotamer: with the exception of $^{1}S_5$, all skew boats appear as intermediates (see Supplementary Material). The inversion of **2d** also depends of the rotamer involved. That of conformer a (Table 2) shows $^{1}S_3$ as the most stable equatorial conformer, but $^{2}S_O$ as the intermediate connected with $^{4}C_1$, and $^{O}S_2$ as that connected with $^{1}C_4$ with less activation energy (Figs. 4 and 5). For conformers b/c, $^{1}S_3$ and $^{O}S_2$ are the lower energy equatorial conformers, and also those connecting with the chairs with lower energy. An alternate connection between $^{4}C_1$ and $^{5}S_1$ is also observed (Fig. 5).

4. Conclusions

The present study has evaluated, by theoretical methods, the three steps necessary for the alkaline transformation of 6-sulfated (and 2,6-disulfated) galactose units into 3,6-anhydro derivatives, a reaction usually carried out at high temperatures. Results show that, as expected, the final substitution step is the rate limiting, involving an activation energy of ca. 23 kcal/mol. The other two steps combined, i.e. deprotonation and chair inversion involve much lower activation energies (9–12 kcal/mol), probably achievable at room temperature. Comparison of the thermodynamics and kinetics of the reactions suggest that if the deprotonation step precedes the chair inversion, the reaction should go faster for both compounds. No major differences in reaction rate can be theoretically predicted to be caused by the presence of sulfate on O-2, although one experimental result suggested that O-2 sulfation should increase the reaction rate. The conformational pathways are complex, given the large number of rotamers available for each compound, and the way that some of these rotamers combine into some of the pathways.

Acknowledgments

This work was supported by grants from UBA (Q203) and CONICET (PIP 0559/10). D.A.N. and C.A.S. are Research Members of the National Research Council of Argentina (CONICET).

Appendix: Supplementary material

Supplementary data to this article can be found online at doi:10.1016/j.carres.2016.03.014.

References

1. Stortz CA, Cerezo AS. *Curr Top Phytochem* 2000;**4**:121–34.
2. Percival EJV. *Q Rev* 1949;**3**:369–84.
3. Rees DA. *J Chem Soc* 1961;5168–71.
4. Ciancia M, Noseda MD, Matulewicz MC, Cerezo AS. *Carbohydr Polym* 1993;**20**:95–8.
5. Hegedüs C, Madarás J, Guyás H, Szöllösy A, Bakos J. *Tetrahedron Asymmetry* 2001;**12**:2867–73.
6. Smidsrød O, Larsen B, Pernas AJ, Haug A. *Acta Chem Scand* 1967;**21**:2585–98.
7. Navarro DA, Stortz CA. *Carbohydr Res* 2003;**338**:2111–8.
8. Freile-Pelegrín Y, Murano E. *Bioresour Technol* 2005;**96**:295–302.
9. Ciancia M, Matulewicz MC, Cerezo AS. *Carbohydr Polym* 1997;**32**:293–5.
10. Viana AG, Noseda MD, Duarte MER, Cerezo AS. *Carbohydr Polym* 2004;**58**:455–60.
11. Noseda MD, Cerezo AS. *Carbohydr Polym* 1995;**26**:1–3.
12. Noseda MD, Viana AG, Duarte MER, Cerezo AS. *Carbohydr Polym* 2000;**42**:301–5.
13. Navarro DA, Stortz CA. *Carbohydr Polym* 2005;**62**:187–91.
14. Imberty A, Pérez S. *Chem Rev* 2000;**100**:4567–88.
15. Kirschner KN, Yongye AB, Tschampel SM, González-Outeiriño J, Daniels CR, Foley BL, et al. *J Comput Chem* 2008;**29**:622–55.
16. French AD, Kelterer A-M, Johnson GP, Dowd MK, Cramer CJ. *J Comput Chem* 2001;**22**:65–78.
17. Kohn W, Becke AD, Parr RG. *J Phys Chem* 1996;**100**:12974–80.
18. Momany FA, Willett JL. *Carbohydr Res* 2000;**326**:210–26.
19. Csonka GI. *J Mol Struct (Theochem)* 2002;**584**:1–4.
20. Appell M, Strati GL, Willett JL, Momany FA. *Carbohydr Res* 2004;**339**:537–51.

21. Csonka GI, French AD, Johnson GP, Stortz CA. *J Chem Theory Comput* 2009;**5**:679–92.
22. Csonka GI, Kaminsky J. *J Chem Theory Comput* 2011;**7**:988–97.
23. Goerigk L, Grimme S. *J Chem Theory Comput* 2011;**7**:291–309.
24. Colombo MI, Rúveda EA, Gorlova O, Lalancette R, Stortz CA. *Carbohydr Res* 2012;**353**:79–85.
25. Sameera WMC, Pantazis DA. *J Chem Theory Comput* 2012;**8**:2630–45.
26. Zhao Y, Truhlar DG. *Org Lett* 2006;**8**:5753–5.
27. Zhao Y, Truhlar DG. *Theor Chem Acc* 2008;**120**:215–41.
28. Tomasi J, Mennucci B, Cammi R. *Chem Rev* 2005;**105**:2999–3093.
29. Frisch MJ, Trucks GW, Schlegel HB, Scuseria GE, Robb MA, Cheeseman JR, et al. Gaussian 09W, Revision B.01. Gaussian Inc., Wallington CT; 2009.
30. Allinger NL, Yuh YH, Lii J-H. *J Am Chem Soc* 1989;**111**:8551–66.
31. Stortz CA. *J Comput Chem* 2005;**26**:471–83.
32. Stortz CA. *J Phys Org Chem* 2010;**23**:1173–86.
33. Peng C, Schlegel HB. *Isr J Chem* 1993;**33**:449–54.
34. Cremer D, Pople JA. *J Am Chem Soc* 1975;**97**:1354–8.
35. Engelsen SB, Koca J, Braccini I, Hervé du Penhoat C, Pérez S. *Carbohydr Res* 1995;**276**:1–29.
36. Ionescu AR, Bérces A, Zgierski MZ, Whitfield DM, Nukada T. *J Phys Chem A* 2005;**109**:8096–105.
37. Hendrickson JB. *J Am Chem Soc* 1967;**89**:7047–61.
38. French AD, Brady JW. *ACS Symp Ser* 1989;**430**:1–19.
39. Smith BJ. *J Phys Chem A* 1998;**102**:3756–61.
40. Joshi NV, Rao VSR. *Biopolymers* 1979;**18**:2993–3000.
41. Dowd MK, French AD, Reilly PJ. *Carbohydr Res* 1994;**264**:1–19.
42. Mayes HB, Broadbelt LJ, Beckham GT. *J Am Chem Soc* 2013;**136**:1008–22.
43. Biarnés X, Ardèvol A, Planas A, Rovira C, Laio A, Parrinello M. *J Am Chem Soc* 2007;**129**:10686–93.
44. Ardèvol A, Biarnés X, Planas A, Rovira C. *J Am Chem Soc* 2010;**132**:16058–65.
45. Plazinski W, Drach M. *RSC Adv* 2014;**4**:25028–39.